Multispectral thermal infrared mapping of sulfur dioxide plumes: A case study from the East Rift Zone of Kilauea Volcano, Hawaii

V. J. Realmuto
Jet Propulsion Laboratory, California Institute of Technology
M.S. 168-514
4800 Oak Grove Drive
Pasadena, CA 91109
818-354-1824 (voice)
818-393-6962 (fax)
Vince.Realmuto@jpl.nasa.gov

A. J. Sutton, and T. Elias
USGS Hawaiian Volcano Observatory
Hawaii Volcanoes National Park, HI 96718

23 October 1996

Abstract

The synoptic perspective and rapid mode of data acquisition provided by remote sensing are well--suited for the study of volcanic SO_2 plumes. In this paper we describe a plume-mapping procedure that is based on image data acquired with NASA's airborne Thermal Infrared Multispectral Scanner (TI MS). We also describe the application of the procedure to TI MS data collected over the East Rift Zone of Kilauea Volcano, Hawaii, on September 30, 1988. These image data covered the Pu'u 'O'o and Kupaianaha vents and a skylight in the lava tube that was draining the Kupaianaha lava pond. Our estimate of the SO_2 emission rate from Pu'u 'O'o (17 -20 kg S-l) is roughly twice the average of estimates derived from COSPEC measurements collected 10 days prior to the TIMS overflight (10 kg S-l). The agreement between the TIMS and COSPEC estimation techniques improves when we compare SO_2 burden estimates, which are relatively independent of wind speed. The potential benefits of this new plume mapping procedure to volcano monitoring programs will be more fully realized when inexpensive data are available on a repetitive basis. In anticipation of the 1998 launch of the Advanced Spaceborne Thermal Emission and Reflectance Radiometer (ASTER), we demonstrate the use of ASTER data to map Pu'u 'O'o - scale SO_2 plumes from space.

Introduction

Andres and Rose [1995] provide an excellent review of the applications of SO_2 emission rate measurements to volcanological research and monitoring. These applications include the estimation of magma supply rates [e.g., *Andres et al., 1991; Casadevall et al., 1981, 1983; Chartier et al., 1988],* contributions of volcanoes to the global SO_2 budget [e.g., *Berresheim and Jaeschke,*

1993; *Kyle et rd.,* 1994; *Stoiber et al., 1987],* and emission rates of other constituents of volcanic plumes [e.g., *Kyle et al.,* 1990; *Rose et al.,* 1986, 1988; *Zreda-Gostynska and Kyle, 1993].*

The introduction of the portable correlation spectrometer, or COSPEC [*Moffat and Millán,* 197 1; *Newcomb and Millán,* 1970], greatly facilitated the measurement of volcanic SO_2 emission rates. The versatility of these spectrometers, which convert measurements of the ultraviolet sky-light transmitted through a plume into estimates of its SO_2 burden, is evident from the number of publications that cite COSPEC measurements [e.g., *Allard et al., 1991; Andres et al., 1989, 1991,* 1993a, 1993b; *Caltabiano et al., 1994; Casadevall et al., 1981, 1983, 1987; Chartier et al., 1988; Doukas and Gerlach, 1995; Kyle et al.,* 1994; *McGee, 1992; Malinconico, 1979, 1987; Stoiber et al., 1983, 1987].*

Although SO_2 emission rates have been measured at a variety of volcanoes [*Andres and Rose, 1995;* Stoiber et al., 1983], relatively few long-term monitoring programs have been documented in the literature. The programs in place at Mount Erebus [*Kyle et al.,* 1994], Mount Etna [*Caltabiano et al., 1994],* Kilauea Volcano [*Casadevall et al., 1987; Chartier et al., 1988; Elias et al., 1993],* and Mount St. Helens [*Casadevall et al., 1983; McGee, 1992; McGee and Sutton, 1994]* have clearly demonstrated the benefits of frequent SO_2 emission rate measurements,

The comprehensive data set from Mount Erebus has revealed that the SO_2 emissions rates are correlated with the surface area of lava lakes, thus allowing investigators to estimate emission rates when no COSPEC measurements are available [*Kyle et al.,* 1990, 1994]. Cyclic variations have been discovered in the rates of SO_2 emission from Mount Etna, where eruptions have been preceded by drops in emission to levels 5 times lower than the base line rate (64 kg S-l, or 5500 metric tons per day) and paroxysmal eruptions have resulted in rates 2 to 5 times higher than the

base line [*Caltabiano* e? *al.,* 1994], COSPEC measurements of SO_2 emissions from Mount St. Helens between 1980 and 1982 showed that while exogenous dome-building events were accompanied by emission rates two to four times higher than those measured between events, there was an overall decline in the base line emission rate over the period of observation [*Casadevall* et cd., 1983]. Based on an analysis of airborne COSPEC and ground-based reducing gas sensor data collected at St. Helens between 1984 and 1988, McGee *and Sutton* [1994] concluded that all of the exogenous dome-building events of this period were preceded by increases in gas emissions.

The collection of such frequent $S0_2$ emission rate measurements can involve considerable labor, expense, logistical planning, and risk to personnel and equipment. Satellite-based remote sensing, which offers synoptic viewing, rapid data acquisition, and repeated observations, might enable volcanologists to obtain frequent estimates of $S0_2$ emission rate at a greater number of volcanoes in a safe and cost-effective manner.

The ability to map the $S0_2$ content of volcanic plumes and clouds from space was first demonstrated by *Krueger [1983],* using data acquired by the Total Ozone Mapping Spectrometer (TOMS)[*Krueger* et *al.,* 1995]. The daily global coverage provided by TOMS has been particularly useful in tracking the stratospheric $S0_2$ clouds formed by large, explosive eruptions [e.g., *Bluth et al.,* 1992, 1994, 1995; *Doiron et al., 1991; Krueger, 1983; Krueger et al., 1990]* and in estimating the contribution of explosive volcanism to the global atmospheric $S0_2$ budget [*Bluth* e? *al.,* 1993; Pyle *et al.,* 1996]. However, the coarse spatial resolution of TOMS (50 km at nadir) has precluded the detection of quiescent $S0_2$ plumes in the troposphere and there have been few applications of TOMS data to the monitoring of non-explosive eruptions [e.g.. *Casadevall et al., 1984; Walter et al., 1993].*

Realmuto et al. [1994] recently demonstrated that image data acquired by NASA's airborne Thermal Infrared Multispectral Scanner (TIMS) could be used to estimate the SO_2 content of volcanic plumes. In this paper we describe a procedure to create two-dimensional maps of SO_2 plumes, and apply the mapping procedure to TIMS data acquired over the East Rift Zone of Kilauea Volcano (Fig. 1). We also discuss the extension of the mapping procedure to the data anticipated from the Advanced Spaceborne Thermal Emission and Reflectance Radiometer (ASTER) [*Kahle et al.*, 1991], which is scheduled for launch in 1998 aboard the first of NASA'S Earth Observing System satellites.

The Plume Mapping Procedure

The plume mapping procedure is an extension of the SO_2 estimation procedure introduced by *Realmuto et al. [1994]. The* estimation procedure operates on a single picture element, or pixel, of image data. The mapping procedure allows us to estimate the SO_2 over blocks of contiguous pixels, thus creating a two-dimensional map of a plume.

The estimation procedure is based on the MODTRAN radiative transfer code [*Berk et al.*, 1989], which we use to model the thermal infrared (TIR) radiance observed by TIMS as it views the ground through an intervening SO_2 plume. MODTRAN calculates atmospheric transmission and radiance using models of the absorption bands of twelve gas molecules (H_2O, CO_2, O_3, N_2O, CO, CH_4, O_2, NO, SO_2, NO_2, NH_3, and HNO_3), utilizing 3-parameter band models with spectral resolutions of 1 cm-l.

Typically an SO_2 plume is cooler than the ground, and we observe the absorption of ground radiance by the plume. The strength of this absorption is a nonlinear function of many

factors, including the concentration of SO_2, thickness of the plume, temperature contrast between the plume and ground, and atmospheric pressure at the altitude of the plume. None of these model parameters are uniquely determined by the TIMS radiance measurements, so the estimation of SO_2 concentrations from radiance measurements is a nonlinear, underdetermined inverse problem.

To create a more tractable inverse problem, we obtain information regarding the plume and surrounding atmosphere from ancillary sources. The net effect of this additional information is to reduce the number of model parameters to (1) ground temperature and (2) S 0_2 concentration. The resulting inverse problem is still underdetermined, since many combinations of temperature and concentration will produce the same fit to an observed radiance spectrum,

Figure 2 contains the spectral response functions for the six TIMS channels, together with the atmospheric absorption that results from the presence of SO_2 in an optical path, To achieve a unique solution to the inverse problem, we make use of the spectral resolution of TIMS to estimate the ground temperature and SO_2 concentration in separate steps. We first estimate the ground temperature beneath a plume by fitting the radiance observed in Channels 4, 5, and 6, which are not affected by SO_2 absorption (Fig. 2). We then use the temperature estimate to find the SO_2 cone-entration that yields the best least-squares fit to the radiance observed in Channels 1,2, and 3, which span the SO_2 absorption features. The temperature estimation requires no iteration, where-s the SO_2 estimation can require a large number of iterations.

Given that we must estimate SO_2 levels at thousands of pixel locations to create a plume map, it is not practical to run MODTRAN at every iteration in the estimation of SO_2. The current version of the procedure requires only six runs of MODTRAN per pixel, The first run, in which the SO_2 concentration is set to zero, is used to estimate ground temperature. The next five runs

increment the SO_2 concentration to a user-specified maximum value. The results of all six runs are used to define the radiance reaching the sensor as a piecewise linear function of SO_2 concentration, and this function is used in the least-squares fitting of the observed radiance spectra.

inputs to the Mapping Procedure

The plume mapping procedure is implemented through a graphical user interface. The user delineates a portion of a plume by drawing a rectangular area of interest on an index image, and the. radiance spectra corresponding to pixels located within the region are input to the SO_2 estimation procedure. This delineation process eliminates the wasted effort of estimating SO_2 in portions of the scene that are obviously free of plumes.

The graphical interface is also used to assign an emissivity spectrum to a region of interest. After identifying the surface material beneath the plume, the user draws a second region of interest *over* an exposure of the same material that is not obscured by the plume. An average emissivity spectrum is calculated from the spectra corresponding to pixels located within this second region, In our experience, an emissivity spectrum averaged over a larger region of interest is preferable to one averaged over a smaller region.

The radiance and emissivity data sets are input to the mapping procedure in image format. Deriving the radiance, emissivity, and index images from the same TIMS data assures that these images will be in spatial registration. Images derived from different data sets can be registered via geometric transformation prior to use in the mapping procedure, but this approach invariably degrades the spatial resolution of the data.

Altitude profiles of atmospheric pressure, temperature, and relative humidity are required inputs to the mapping procedure. These profiles are typically measured with balloon-borne radiosondes or derived from climatological records. Assuming that the passive, or horizontal, portion of a plume is in equilibrium with the atmosphere, the pressure, temperature, and relative humidity of the plume are defined by the atmospheric profiles.

Additional inputs include the plume dimensions (defined by midpoint altitude and thickness), altitude of the aircraft/sensor, and elevation of the ground beneath the plume. The ground elevation may be defined by a digital elevation model (DEM), which must be in registration with the index image, or input manually. The plume dimensions, ground elevation, and sensor altitude are used to resample the atmospheric profiles into new profiles which emphasize the medium between the sensor and ground.

Ground elevation and observed radiance are the only inputs that can vary once plume mapping has begun within a region of interest, and the variation in elevation is only possible if a DEM has been submitted to the mapping procedure. The size of a region of interest is therefore proportional to the uniformity of the plume dimensions and the homogeneity and topographic relief of the ground beneath the plume. Mapping a laminar plume over a homogeneous, low-relief background, such as a large body of water, would require a small number of large regions. Mapping an irregular plume over a heterogeneous, high-relief background would require a large number of small regions.

The East Rift Zone Demonstration Site

We applied the mapping procedure to TIMS data acquired over the East Rift Zone (ERZ) of Kilauea Volcano on 30 September 1988. Plume mapping was not the original objective of this airborne survey, so the dimensions and SO_2 contents of the plumes and the local atmospheric conditions were not measured at the time of the overflight, Despite the lack of these ancillary measurements, the ERZ data set was well suited for a demonstration of the mapping procedure. There were at least three distinct SO_2 plumes present at the time of the TIMS overflight, and the gentle relief and uniform lithology of the Kilauea shield provided a relatively simple background to these plumes.

Our demonstration site is located in the middle portion of the ERZ, approximately 21 km E of the summit of Kilauea, and 37 km S of the town of Hilo (Fig. 1). This portion of the ERZ cent ains the Pu ‘u ‘ O’o and Kupaianaha vents, which were the sources of two of the S 0_2 plumes imaged during the airborne survey. *Realmuto et* al. [1992] provide a description of volcanic activity at the ERZ site at the time of this survey.

The TIMS data were acquired during Episode 48 of the Pu‘u ‘O ‘o - Kupaianaha eruption of Kilauea. This eruption began in January, 1983 [cf. *Wolfe et al.,* 1988], and continues as of this writing (October, 1996). Episode 48 began in July, 1986, with the opening of the Kupaianaha vent and ended in February, 1992, with the cessation of magma flow to this vent. *Heliker and Wright [1991], Mattox et al. [1993], Hon et al, [1994],* and *Mangan et al.* [1995] describe events that occurred during this long-lived episode.

Pu'u '0'0 Emission Rates

Several workers have reported on the rates of SO_2 emission from Pu'u 'O'o during various episodes of the eruption. *Casadevall et* al. [1987] measured the emission rates over periods spanning Episodes 6-9 (1983) and 14-28 (1984). The rates measured during the episodes were in the range of 59 to 370 kg s^{-1} (5100 -32,000 t d^{-1}), while those measured between episodes ranged between 0.23 and 3.0 kg s^{-1} (20 -260 t d^{-1}). *Chartier et al. [1988]* measured an average emission rate of 1.9 ± 0.96 kg S-l (167 ± 83 t d-l) between June 13 and July 6, 1985, which was a period of repose between Episodes 33 and 34.

Andres et al. [1989] measured the combined flux from Pu'u 'O 'o and Kupaianaha via vehicle-mounted COSPEC surveys. Between October 14 and November 3, 19S6, the average SO_2 emission rate was 14 ± 4.6 kg s^{-1} (1170 ± 400 t d^{-1}). They estimated that two-thirds of the flux was contributed by Pu 'u 'O' o, and one-third was contributed by Kupaianaha.

The USGS Hawaiian Volcano Observatory (HVO) continues to measure the rates of S02 emission from Pu'u 'O'O [*Elias et al.,* 1993; *Sutton et al.,* 1993]. Between October 29, 19S7, and September 13, 1989, the average emission rate from Pu'u 'O'o (based upon the unpublished data from 18 COSPEC campaigns) was 9.7 ± 2.3 kg s^{-1} (840 ± 202 t d^{-1}). The highest and lowest rates measured during this period were 14.5 and 5.8 kg s^{-1} (1255 and 504 t d-]), respective y. The average emission rate over the nine COSPEC surveys conducted in 1988 was 10.6 ± 2.3 kg S-l (920 ± 200 t d-l), with high and low rates of 14.5 and 7.8 kg s^{-1} (1255 and 670 t d-]), respectively.

The NASA airborne survey of the ERZ took place ten days after an HVO COSPEC survey of Pu'u 'O'o on September 20, 1988. The average emission rate over the 3.5 hour period of measurement was 9.6 ± 2 kg s^{-1} (831 ± 170 t d^{-1}).

Spectral Properties of SO_2 Plumes and Meteorologic Clouds

Our analysis of the TIMS data from the ERZ incorporated NS001 image data, which were acquired simultaneously with the TIMS data. The NS001 scanner measures scene radiance in seven spectral channels between 0.4 and 2.2 μm. The NS001 data were used to estimate the dimensions of the plumes (Table 1), based on the cloud shadows and solar zenith and azimuth angles (50.5° and 111.5°, respectively), and to discriminate the SO_2 plumes from meteorologic clouds. Such discrimination is important, since we do not account for such clouds in our SO2 estimation procedure.

Plate 1 depicts the SO_2 plumes that originated from Pu'u 'O'o, Kupaianaha, and a skylight, or opening, in the roof of the lava tube that was draining the Kupaianaha lava pond. These data were acquired at approximately 9:10 HST (19:10 UT) from an altitude of 1.9 km (roughly 1 km above ground level) which resulted in data with a spatial resolution of approximately 3 m.

Plate la is a color-composite of imagery from NS001 Channels 1, 2, and 3, which are located in the visible portion of the electromagnetic spectrum (0.4 to 0.7 pm). Plate 1 b is a color-composite of the short-wave infrared (SWIR) imagery from NS001 Channels 7 (2.10 -2.38 pm), 6 (1 ,57-1.71 pm), and 5 (1. 13-1.35 μm) displayed in red, green, and blue, respectively. When illuminated by visible radiation (Plate la) the volcanic plumes are similar in appearance to the overlying meteorologic clouds. Under SWIR illumination (Plate lb) the plumes appear in translucent blue colors, but there is little change in the appearance of the clouds relative to Plate 1a.

This discrimination of plumes from clouds makes use of the scattering properties of water droplets, the major constituent of these bodies, and differences in the thickness of the plumes and

clouds. For a given droplet size, the scattering efficiency of a volume of water droplets is inversely proportional to the wavelength of the incident energy [cf. *Stephens,* 1994; *Bohren and Huffman, 1983]. The* SO_2 plumes appear opaque in Plate la due to efficient scattering of the incident visible radiation, and they appear translucent in Plate lb due to diminished scattering of the incident SWIR radiation.

The pale blue coloration of the plumes in Plate 1 b results from the increased amount of scattering of radiation in NS001 Channel 5, which covers the shortest wavelengths of the SWIR channels used to make the color composite, relative to the scattering in Channels 6 or 7. Although the incident SWIR energy penetrated deeper into the clouds than the visible energy, the central portions of the clouds were thick enough to attenuate the SWIR energy and remain opaque in Plate 1 b. The thin margins of the clouds behaved in much the same manner as the plumes, and appear in translucent blue in the SWIR color-composite.

Plate 2 is a color-composite of image data from TIMS Channels 5, 3, and 2 (Fig. 2) displayed in red, green, and blue, respectively. These data were processed to depict temperature variations as changes in the brightness of the display colors (brighter colors signifying warmer temperatures) and spectral variations as changes in the hue and saturation of the display colors [cf. *Gillespie et al., 1986].* The absorption of ground radiance in Channel 2 causes the SO_2 plumes to appear in hues of yellow and red in this color-composite.

Scattering is negligible in the TIR, so we must identify the clouds and plumes from absorption or emission features. Water vapor, which is abundant in the lower atmosphere as well as in c1 ouds and plumes, absorbs (and therefore emits) radiation in the TIR [cf. *Stephens,* 1994; *Goody and Yung,* 1989]. If a cloud is cooler than the ground beneath it, the presence of that cloud

in a TIMS scene is usually revealed by an apparent cooling of the ground, However, a comparison of Plates 1 and 2 indicates that these ground cooling effects can be quite subtle. The difficulty in recognizing clouds in the TIMS data underscores the importance of using the NS001 data to identify portions of the SO_2 plumes that were overlain by clouds.

East Rift Zone Plume Maps

Plates 3 and 4 are SO_2 column abundance (the product of SO_2 concentration and plume thickness) and ground temperature maps, respectively, of the Pu'u 'O'o plume. Plates 5 and 6 are the corresponding maps of the Kupaianaha and skylight plumes. Each color contour map has been shaded to facilitate the visualization of structure in the spatial distributions of the column abundance and ground temperature estimates. The column abundance maps also feature the transect lines across which we calculated SO_2 emission rates.

Any interpretation of a column abundance map must include a comparison with the corresponding ground temperature map. Since SO_2 concentration and ground temperature are the only free parameters in the estimation procedure, all of the accumulated error will be mapped into the estimates of these parameters. Overestimation of ground temperature results in an apparent increase in the temperature contrast between the plume and ground, which can lead to overestimation of SO_2 concentration. By reducing the apparent thermal contrast, underestimation of ground temperature can lead to underestimation of SO_2 concentration. Although accurate ground temperature estimates do not guarantee accurate SO_2 concentration estimates, anomalous ground temperature estimates are indicative of erroneous SO_2 estimates.

input Parameters

We generated the index, radiance, and emissivity images of Pu'u 'O'o and Kupaianaha from the TIMS data set depicted in Plate 2, using the techniques discussed in *Realmuto et al. [1992]*. Table 1 lists the plume dimensions derived from the cloud shadow measurements. Ground elevation values were input manually, since we did not have a DEM that matched the high spatial resolution (3 m) of the image data. The lack of a DEM was of little consequence given the gentle relief of the Kilauea shield in the vicinity of the vents.

Profiles of atmospheric pressure, temperature, and relative humidity over the island of Hawaii are measured every twelve hours by the National Weather Service. These measurements are collected by balloon-borne radiosondes launched from Hilo Airport (Fig. 1). The data used to construct our plume maps were acquired during Ascension # 738. This radiosonde was launched at 13:00 HST (23:00 UT), approximately 4 hours after the NASA overflight of the ERZ.

Pu'u 'O'o Plume Maps

The Pu'u 'O'o column abundance map (Plate 3) shows that the distribution of SO_2 within the plume was not uniform. The SO_2 column abundance ranged between 16 and >32 g m^{-2} for the high-concentration puffs entrained within the plume. The abundance ranged between 2 and 8 g rn^{-2} outside of these puffs.

A comparison of the column abundance and ground temperature maps (Plates 3 and 4, respectively) indicates that the temperature estimates were generally more sensitive to the texture of the ground than to the SO_2 concentration of the plume. The rough surface of an aa flow enhances aerodynamic cooling, and aa flows appear cooler than glassy pahoehoe flows in the.

temperature maps, The exceptions to this general observation are marked as temperature anomalies in Plate 4.

The northern temperature anomalies are associated with the puffs intersected by Transects A and B (Plate 3). The anomalous ground temperatures are 1-3 K cooler than the surrounding temperatures, and are probably the result of water vapor in the puffs that was not present in the atmospheric profile. Alternatively, the puffs may have been thicker than our specification to the estimation procedure (Table 1). The small magnitude of the temperature anomalies, together with the observation that the anomalously cool regions were less than a third of the size of the corresponding puffs, offer little evidence that the S 0_2 concentration estimates within the puffs are not accurate.

The southern temperature anomalies (Plate **4) are** clearly associated with the southernmost puffs (Plate 3). These ground temperatures are 5- 8 K cooler than the surrounding temperatures and the anomalous regions are roughly the same size as the corresponding puffs. A comparison of Plates 1 and 4 indicates that the southern anomalies were probably the result of occultation of the plume beneath thin tendrils of a meteorologic cloud. While the radiance spectra from the obscured portions of the plume did exhibit $S0_2$ absorption features, the water vapor in the cloud caused anomalously low ground temperature estimates. We conclude that the $S0_2$ concentration estimates are also in error, and we exclude the southern puffs from our estimation of emission rates.

Kupaianaha Plume Maps

Prior to the generation of the Kupaianaha plume maps (Plates 5 and 6) we added a binning algorithm to the mapping procedure. The strategy of this algorithm is to reduce the number of

times the estimation procedure is run within a region of interest. New runs of the procedure are limited to pixels with zenith angles (which define the optical path between the ground and sensor), ground elevations, and radiance spectra that are significantly different from those of pixels processed by prior runs of the procedure. The estimation procedure will return the same ground temperature and SO_2 estimates at pixels that share these attributes.

The locations of unique pixels are stored in an array of bins, and the attributes of each new pixel are compared with those of the binned pixels, If the differences between the attributes are greater than user-defined tolerance levels, the new pixel is considered to be unique, the estimation procedure is run, and the location of the pixel is added to the bin array. Non-unique pixels are assigned the SO_2 and temperature estimates from a similar pixel in the bin array. The time required to compare each new pixel to those in the bin array can become a liability if a large number of heterogeneous pixels are to be mapped. In such cases the user can override the binning algorithm by setting the tolerance levels to zero.

The Kupaianaha column abundance map (Plate 5) shows that this plume was also composed of puffs, albeit at lower SO_2 levels than in the Pu'u 'O'o plume (Plate 3). SO_2 column abundances within the Kupaianaha puffs ranged between 5 and 8 g m^{-2}. The skylight plume was discontinuous and weak, with maximum abundances of less than 6 g m^{-2}.

There are no indications of anomalous ground temperatures in the Kupaianaha temperature map (Plate 6). The largest puff in the Kupaianaha plume, intersected by Transect A (Plate 5), was situated over a contact between pahoehoe and aa flows. A comparison of Plates 5 and 6 reveals that the 8 - 10 K change in the ground temperature estimates did not affect the corresponding SO_2 column abundance estimates. Virtually all of the large changes in ground temperature were

aligned with contacts between different surface materials, further demonstrating the influence of surface texture on ground temperature.

Discussion

Sources of Error

The accuracy of the mapping procedure is a function of the accuracy of the radiance measurements, approximations made in the estimation procedure, and description of the transfer of radiation from ground to sensor. Our ability to describe this transfer depends on our knowledge of the plume dimensions (altitude and thickness), atmospheric conditions, and ground emissivity [cf. *Realmuto et al.,* 1994]. The potential sources of error are discussed below.

Sensitivity and Accuracy of TIMS. A laboratory calibration of TIMS conducted in December of 1987 indicated that the sensitivities of Channels 1 through 5 were better than 0.2 K, while Channel 6 was rated at better than 0.35 K. Instrument sensitivity, known as the noise-equivalent change in temperature (NEAT) or smallest change in temperature that can be detected in the presence of system noise, is more closely related to precision than accuracy. Our experience with in-flight calibration experiments of TIMS suggests that the accuracy of the 1988 data was probably between ± 2 and 5 K.

Approximation Errors. Tests of the estimation procedure with synthetic data indicate. that our use of a piecewise linear function in the estimation procedure can result in overestimates of S02 concentrations of up to 10%. The errors appear to be independent of the actual $S0_2$ concentration and the maximum concentration used to generate the function.

Tests of the binning algorithm indicate that the number of pixels at which the estimation procedure is run can be reduced by a factor of two, Approximately 90% of the resulting SO_2 estimates were within ± 10% of the estimates obtained without binning, and there was no appreciable bias (less than -1%) in the binned SO_2 estimates.

Plume **Dimensions.** In our estimation of the altitude and thickness of the plumes from cloud shadows, we found that the most difficult aspect of this technique was the identification of points on a cloud that were responsible for the corresponding points on a shadow. To combat this problem, we obtained a range of elevations and thicknesses for a given plume and used the midpoints of these ranges as the plume dimensions. The results of this exercise suggest errors in our plume dimensions of ±10% are possible, if not probable.

Given our lack of direct observations of the dimensions of the plumes, we assumed that the plumes were laminar over the region covered by the image data. While this assumption may be generally valid, it is likely that the puffs were of different thicknesses. Since plume thickness is a fixed parameter in the estimation procedure, any differences in the thicknesses of the three puffs in the Pu 'u 'O' o plume (Plate 3) were mapped as differences in S 0_2 concentrations.

Local Atmospheric Conditions. We assumed that the plumes were in equilibrium with the local atmosphere, and that the temperature, pressure, and relative humidity of a plume were defined by the Hilo radiosonde data. The ability of these measurements to describe the local atmospheric conditions at the ERZ study site is suspect, given that the radiosonde was launched from a distant site four hours after the airborne survey was concluded. The ground temperature estimates (Plates 4 and 6), which are indicative of the accuracy of the atmospheric data, appear to

be reasonable. However, any attempt to quantify the temperature estimation errors is limited by our lack of independent ground temperature estimates made at the time of the overflight.

Our assumption that the water vapor content of a plume was described by the radiosonde data implies that any H_20 exsolved from the Pu 'u 'O'o magma column had condensed into waler droplets downwind of the vent. This hypothesis is supported by the lack of any distinct spectral anomalies in the SWIR and TIR imagery of the ERZ plumes (Plates 1 and 2), together with the reasonable ground temperature estimates (Plates 4 and 6), but we have little doubt that the radiosonde measurements did not account for all of water vapor in the Pu'u 'O'o plume.

The Hilo radiosonde recorded a temperature inversion between the altitudes of 1,4 and 2.4 km. It is possible that the Pu'u 'O'o plume was a buoyant plume trapped beneath this inversion layer [cf. McGee, 1992], rather than a passive plume in equilibrium with the local atmosphere, but it is probable that the wind velocity was too high to allow the plume to pool beneath any inversion layers.

Error Budget. Although we cannot quantify all of the errors discussed above, we can estimate a minimum error budget for the mapping procedure. Taking the square root of the sum of the squares of the error resulting from uncertainties in the accuracy of TI MS, piecewise linear approximation, binning algorithm, and plume dimensions, we arrive at an error budget of ±17%.

Sensitivity Analysis

Given the dependence of the estimation procedure on data that are ancillary to the radiance measurements, we have evaluated the sensitivity of the $S0_2$ estimates to our knowledge of the atmospheric profiles, plume dimensions, and ground elevation. The measurement of atmospheric

profiles or plume dimensions typically requires that scientists be in the field at the time of the sensor overflight, and this presence may not be safe or practical in many field settings. The input of accurate ground elevations requires accurate topographic maps or DEMs, which will not be available for every volcano of interest.

To evaluate the sensitivity of the estimation procedure to our knowledge of the atmospheric pressure, temperature, and relative humidity profiles, we replaced the Hilo radiosonde data with a model of a tropical atmosphere and recreated a portion of the Pu' u 'O 'o plume map. The tropical model is integral to MODTRAN, which contains model atmospheres for a variety of latitudes and seasons. We processed a block of 100 pixels centered on the puff intersected by Pu'u 'O'o Transect B (Plate 3).

Our comparison of this test segment with the original plume map suggests that the $S0_2$ estimates are not very sensitive to the atmospheric profiles. The change in the $S0_2$ column abundance was less than 10% for over 90% of the pixels in the test segment, with changes between 6 and 8% observed for the majority (55%) of the pixels.

To evaluate the sensitivity of the estimation procedure to our knowledge of the plume dimensions, we ran the procedure at a single pixel, located in the puff intersected by Pu'u 'O'o Transect B (Plate 3), while varying the plume (midpoint) altitude and thickness. The dimensions were varied independently, holding one at the value listed in Table 1 while the other was varied. The ranges over which we could vary the plume dimensions were limited by the algorithm for resampling atmospheric profiles, which requires that the difference between the plume altitude and the ground elevation or sensor altitude be greater than or equal to the plume thickness.

Figure 3a shows the change in the estimate of SO_2 that resulted from a change in the plume altitude. We expected that the SO_2 estimates would be sensitive to the plume altitude, as this parameter, together with the profile of atmospheric temperature, defines the temperature of the plume. There was a roughly linear decrease in the SO_2 estimate as the altitude was increased to 1.30 km (18% change, Fig. 3a), due to the apparent increase in the temperature contrast between the plume and ground. The increase in the SO_2 estimate for altitudes above 1.30 km was due to the temperature inversion layer recorded in the Hilo radiosonde data, which reduced the apparent temperature contrast between the plume and ground. Within the broad inversion layer a 10% increase in plume altitude resulted in an increase in SO_2 column abundance of less than 5%.

Figure 3b illustrates that the estimation procedure is relatively insensitive to changes in the plume thickness. Despite reductions in thickness of up to 60%, the reduction in the SO_2 estimate was never greater than 4%.

To evaluate the sensitivity of the estimation procedure to our knowledge of the ground elevation, we ran the procedure at the aforementioned pixel while varying this parameter. The plume dimensions were held constant. There was a monotonic decrease in the SO_2 estimate with a decrease in elevation, but the effect was minimal. A reduction in elevation of 200 m (24%) resulted in a reduction of less than 1.5% in the corresponding SO_2 estimate.

Comparison with COSPEC

The proximity in time of the HVO COSPEC (September 20, 1988) and TIMS (September 30, 1988) surveys of Pu'u 'O'o, combined with the characterization of the variability in Pu'u 'O'o emission rates during this time frame, presents us with a unique opportunity to compare the results

of the TIMS and COSPEC surveys. To estimate emission rates for the transect lines on the plume map (Plate 3), we must first estimate the speed of the wind at the *time* of the TIMS overflight.

The alignment of the plumes in the NSOO1 image data (Plate 1) indicates that the wind was coming from the N. Records from a National Park Service (NPS) meteorology station at the summit of Kilauea indicate that the wind was coming from the NE (41°) at a speed of 5.7 m s^{-1} at the time of the overflight and the average windspeed for the day was 5.6 ± 0,4 m s-l. The summit of Kilauea is located approximate] y 21 km WNW of the ERZ site at an elevation roughly 550 m higher than that of the site, but the NPS wind speed measurements are consistent with the average wind speed measured at Pu'u 'O'o during the COSPEC survey on September 20, 1988 (5.1 ± 0.4 m s^{-1}). Given this consistency, and the stability of the wind speed at Kilauea on September 30, 1988, we assume that the wind speed at the time of the overflight was between 5 and 6 m s-l.

The emission rates derived from the four transects across the Pu'u 'O'o plume map (Plate 3) are listed in Table 2. The average of the four rates ranges between 16.8 and 20.2 kg s^{-1} (1449 - 1741 t d^{-1}), with a standard deviation of 7.1 -8.6 kg s^{-1} (617 -741 t d^{-1}), which is roughly twice the average emission rate measured on September 20, 1988 (9.6 ± 2 kg S-l or831 ± 170 t d^{-1}). Our rate estimate is roughly twice as large as the average rate measured in 1988 (10.6 ± 2.3 kg s^{-1} or 920 ± 200 t d^{-1}) and slightly larger than the highest rate measured that year (14.5 kg s^{-1} or 1255 t d^{-1}). Given the high potential for error in the plume mapping procedure, the favorable comparison between the results of the TIMS and COSPEC surveys is encouraging.

The SO_2 emission rate (mass per unit time) is derived as the product of the wind speed and total SO_2 burden (mass per unit length), which is the integral of a burden profile measured along a transect through a plume in a plane perpendicular to the wind direction Since neither COSPEC nor

TIMS measure emission rates directly, and inaccurate knowledge of wind speed is one of the largest sources of error in derivations of emission rate [*Chartier et al.*, 1986; *Stoiber et cd., 1983],* our comparison of the results of the COSPEC and TIMS surveys should be independent of wind speed.

The COSPEC survey consisted of 29 transects through the plume collected over a period of 3.5 hours, Figure 4 is a plot of the total $S0_2$ burden levels derived from the individual transects. The levels ranged between 1000 and 3000 g m^{-1}, with a mean value of 1771 ± 642 g m^{-1}. The total burden levels derived from the Pu 'u 'O'o plume map transects (Plate 3) are found in Table 2. The levels for Transects A and B, which intersect high-concentration puffs, fall outside of the range defined by the COSPEC measurements (Fig. 4). The levels for Transects C, which does not cross a puff, and D, which intersects the weakest of the puffs, fall within this range. To explain the outcome of this comparison we must examine the differences in the modes of operating COSPEC and TIMS.

The COSPEC transects were collected by panning the field of view of a tripod-mounted instrument in a vertical plane through the plume [cf. *Sutton et al.,* 1992]. Each transect required 3 to 4 minutes to complete. Given the average wind speed on September 20.1988 (5.13 ± 0.4 m s^{-1}), a single high-concentration puff could not have filled the field of view of the COSPEC for an entire transect [cf. *Stoiber et al., 1983].* Therefore, the contributions of the puffs to a burden profile were diluted by the contribution of the low concentration flow that entrained the puffs.

TIMS provided virtually instantaneous and synoptic measurements of the Pu'u 'O'o plume on September 30, 1988. The data depicted in Plate 3 were acquired in approximate y 16 seconds, but the component of wind speed in the flight direction (2.5 -3 m s^{-1}) was small relative to the

ground speed of the aircraft (80 m s^{-1}), and the high-concentration puffs were virtually stationary with respect to the aircraft. Therefore, the burden profiles across the Pu'u 'O'o plume map transects are independent of time. The agreement between the COSPEC total burden levels (Fig. 4) and those of Transects C and D (Table 2), and the disagreement between the COSPEC levels and those of Transects A and B are consistent with a dilution of the contribution of puffs to the COSPEC measurements.

Puffing has been cited as the cause of variations in COSPEC estimates of SO_2 emission rates at a number of volcanoes [cf. *Chartier et al.,* 1988; *Kyle et al., 1994; McGee,* 1992; *Stoiber et al., 1983].* The standard approach to minimizing this effect is to collect a large number of COSPEC transects and calculate the average emission rate over time. Our estimate of the average emission rate is biased, since three of the four Pu 'u 'O 'o transect lines intersect puffs (Plate 3). To avoid such bias, a large number of uniformly-spaced transect lines should be chosen to calculate the average emission rate over space.

Characteristics of the Plumes

We can use the Pu'u 'O'o plume map (Plate 3) to estimate the rate of puffing from this vent at the time of the airborne survey. Given a range of wind speeds between 5 and 6 m s^{-1}, the puffs intersected by Transect D and B were separated by 68-82 seconds, and the puffs intersected by Transects B and A were separated by 37-44 seconds. This rapid rate of puffing contrasts with the 7-45 minute periodicity reported by *Chartier et al. [1988],* suggesting that a different mechanism was responsible for puffing observed during the airborne survey.

A possible source of the puffs may have been the abrupt release of gas from beneath the brittle crust over the Pu 'u 'O'o lava pond. However, observations of this gas piston action in other Kilauean lava lakes indicate periods of tens of minutes *[Swanson et al.,* 1979] to hours [*Tilling,* 1987]. The circulation of magma beneath the thin crust of the pond caused the crust to breakup into plates and vigorous spattering at the margins of plates may have been the source of the puffs. In addition, the release of fumes from Pu'u 'O'o may have been modulated by convecting air cells within the crater. Such cells result from an asymmetric heating of the air mass within the crater due to the location of the lava pond in the northeastern section of the crater floor [T. Gerlach, pers. communication].

Although the principal sources of SO_2 plumes in the Pu'u 'O'o - Kupaianaha system were captured in the image data, there was additional venting from skylights over the 11 km length of the lava tube network [cf. *Realmuto et al., 1992].* Based on the low SO_2 concentrations mapped at the skylight vent (Plate 5), the contribution of the skylights to the SO_2 budget of the system must have been minimal. Summing up the average SO_2 emission rate from Pu'u 'O'o, Kupaianaha, and the skylight (Table 2), we find that Pu'u 'O'o contributed 70% of the total emission from the system, while Kupaianaha and the skylight contributed the remaining 30%. Given the excellent agreement of this ratio with that derived by *A ndres et al. [1989],* the relative contribution of the vents to the total emission appears to have been the same in 1986 and 1988.

Plume Mapping from Space

The use of TIR image data in operational volcano monitoring programs is not feasible, due to the logistics and expense of the airborne mode of data acquisition. This situation may change

with the 1998 launch of NASA's Earth Observing System (EOS) AM-1 platform, which will carry ASTER [cf. *Kahle et al., 1991]* into orbit. The satellite will orbit the Earth 15 times per day and repeat its ground track every 16 days, providing ASTER with the opportunity to collect detailed time-history data sets of volcanic plumes and clouds. ASTER TIR data will have a spatial resolution of 90 m, covering a ground-track swath of 60 km, To compensate for this narrow swath, the ASTER TIR camera can be pointed up to 8.55° from nadir in directions perpendicular to the ground track.

Plate 7 is a version of the Pu'u '0'0 plume map (Plate 3) resampled to the 90 m spatial resolution of ASTER. The four high-concentration puffs can be recognized in the ASTER map, although the concentrations have been diluted (1 O to 16 g m^{-2} column abundance) by the larger footprint of ASTER.

Figure 5 shows the apparent reduction of ground temperature that would be perceived by ASTER if it viewed the ground through the Pu 'u 'O'o plume. This simulation indicates that the temperature reductions due to column abundances of 15 and 10 g m^{-2} will exceed the 0.2- 0.3 K NEAT specified for the ASTER TIR channels, while the reduction due to an abundance of 5 g m^{-2} may be too small to be detected. A comparison of Plate 7 and Figure 5 suggests that the spatial and signal resolution of ASTER will be sufficient to map tropospheric plumes at the scale and altitude of the Pu'u 'O'o plume,

Conclusions and Recommendations

We have described a procedure to map the SO_2 content of volcanic plumes from multispectral TIR imagery. The application of this mapping procedure to image data acquired over the

Pu'u 'O'o and Kupaianaha vents in the ERZ of Kilauea Volcano produced results that are in agreement with near-contemporaneous COSPEC measurements, despite our lack of measurements of the plume dimensions or atmospheric conditions at the time the data were acquired.

The plume dimensions were derived from cloud shadows and the elevation of the ground beneath the plumes was determined from standard topographic maps. We obtained atmospheric profile data from the National Weather Service, although our sensitivity analysis suggested that a standard atmospheric model, derived from climatology, would have been sufficient. None of the procedures or sources used to derive or obtain ancillary data are unique to Kilauea Volcano.

Our sensitivity analyses suggest that errors in the SO_2 estimate can be linearly proportional to errors in the knowledge of plume altitude, since this parameter defines the temperature of the plume. However, uncertainties in the knowledge of plume thickness and ground elevation proved to have little effect on the corresponding $S0_2$ estimates.

Although we have demonstrated that reasonable estimates of SO_2 emission rates can be obtained without the benefit of contemporaneous field measurements, we recommend the combined use of TIR imaging and COSPEC. A comparison of the results of two estimation techniques is often the only practical means of determining the accuracy of either technique. Moreover, the COSPEC can be used to measure the vertical dimensions of the plume that cannot be resolved by the. image data and the image data can be used to extrapolate the localized COSPEC measurements to larger portions of the plume.

The results of the ERZ plume mapping and sensitivity analyses, together with the successful application of the estimation procedure to TIMS image data from Mount Etna [*Realmuto et al., 1994],* indicate that our mapping procedure is a viable, robust, and flexible new tool for the

study of volcanic plumes, The potential benefits of image-based SO_2 mapping to volcano monitoring will be more fully realized when inexpensive data are available on a repetitive basis, and we have demonstrated the feasibility of mapping Pu'u 'O'o-scale SO_2 plumes from space with ASTER data. Under the guidelines of the EOS program, these data, together with the necessary software, will be available to any investigator who wishes to use the plume mapping procedure.

Acknowledgments

We thank our colleagues at the USGS Hawaiian Volcano Observatory for the data, assistance, and cooperation given in support of this research. Thanks also go to the crew of the NASA C-130B aircraft and the staff of the Aircraft Data Facility, both based at the NASA/Ames Research Center. R. Carson of the National Park Service provided the weather station data for Kilauea. We are grateful to R. Holasek for his help with astronomical almanac software. The authors appreciate the thorough reviews of this manuscript by G. Bluth, R. Andres, and an anonymous reviewer. Portions of this research were conducted at the Jet Propulsion Laboratory, California Institute of Technology, under contract to the National Aeronautics and Space Administration.

References

Allard, P., J. Carbonnelle, D. Dajlevic, J. Le Bronec, P. Morel, M. C. Robe, J.M. Maurenas, R. Faivre-Pierret, D. Martin, J. C, Sabroux, and P. Zettwoog, Eruptive and diffuse emissions of $C0_2$ from Mount Etna, *Nature, 351*, 387-391, 1991.

Andres, R. J., P. R. Kyle, J. B. Stokes, and W. 1, Rose, $S0_2$ from episode 48A eruption, Hawaii: sulfur dioxide emissions from the episode 48A east rift zone eruption of Kilauea volcano, Hawaii, Bull. *Volcanol.*, 52, 113-117, 1989.

Andres, R. J., W. I. Rose, P. R. Kyle, S. deSilva, P. Francis, M. Gardeweg, and H. Moreno-Roa, Excessive sulfur dioxide emissions from Chilean volcanoes, *J. Volcano/. Geotherm. Res., 46,323-329, 1991.*

Andres, R. J., P. R. Kyle, and R. L. Chuan, Sulphur dioxide, particle, and elemental emissions from Mount Etna, Sicily, Italy, during July 1987, *Geol. Rundsch, 82,687-695*, 1993a.

Andres, R. J., W. I. Rose, R. E, Stoiber, S. N. Williams, O. Matais, and R. Morales, A summary of sulfur dioxide emission rate measurements from Guatemala volcanoes. *Bull. Volcanol., 55,379-388,* 1993b.

Andres, R. J., and W. I. Rose, Remote sensing spectroscopy of volcanic plumes and clouds, in *Monitoring Active Volcanoes,* edited by B. McGuire, C.R.J. Kilburn, and J. Murray, pp. 301-314, University College London, London, 1995.

Berresheim, H., and W. Jaeschke, The contribution of volcanoes to the global atmospheric sulfur budget, *J. Geophys. Res.,* 88,3732-3740, 1983.

Berk A, L.S. Bernstein, and D. C. Robertson, MODTRAN: a medium resolution model LOWTRAN-7, *GL-TR-89-0122,* 1989.

Bluth, G. J. S., S. D. Doiron, C. C. Schnetzler, A. J. Krueger, and L. S. Walter, Global tracking of the SO_2 clouds from the June 1991 Mount Pinatubo Eruptions, *Geophys. Res. Let., 19, 151-154, 1992.*

Bluth, G. J. S., C. C. Schnetzler, A. J. Krueger, L. S. Walter, The contribution of explosive volcanism to global atmospheric sulphur dioxide concentrations, *Nature, 336,327-329, 1993.*

Bluth, G. J. S., T. J. Casadevall, C. C. Schnetzler, S. D. Doiron, L. S. Walter, A, J. Kreuger, and M. Badruddin, Evaluation of sulfur dioxide emissions from explosive volcanism: the 1982-1983 eruptions of Galunggung, Java, Indonesia, *J. Volcanol. Geotherm. Res., 63,243-256, 1994.*

Bluth G. J. S., C. J. Scott, I. E. Sprod, C. C. Schnetzler, A. J. Krueger, and L. S. Walter, Explosive emissions of sulfur dioxide from the 1992 Crater Peak eruptions, Mount Spurr, Alaska, in *USGS Bull. 2139,* edited by T.E.C. Keith, pp. 47-57, 1995.

Bohren C. F., and D. R. Huffman, *Absorption and Scattering of Light by Small Particles, 530* pp., Wiley-Interscience, New York, 1983.

Caltabiano, T., R. Romano, G. Budetta, SO_2 flux measurements at Mount Etna (Sicily). *J. Geophys. Res., 99, 12,809-12,819, 1994.*

Casadevall, T. J., D.A. Johnston, D. M. Harris, W. I. Rose, L. L. Malinconico, R. E. Stoiber, T, J. Bornhorst, S. N. Williams, L. Woodruff, and J. M. Thompson, SO_2 Emission Rates at Mount St. Helens from March 29 through December 1980, in *USGS Prof. Paper 1250,* *edited* by P. Lipman and D. R. Mullineaux, pp. 193-200, 1981,

Casadevall, T. J., A. J. Krueger, and J. B. Stokes, The volcanic plume from the 1984 eruption of Mauna Loa, Hawaii, *EOS i'bans. AGU,* 65, 1133, 1984.

Casadevall, T. J., W. I, Rose, T. Gerlach, L. P. Greenland, J. Ewert, R. Wunderrnan, and R. Symonds, Gas emissions and the eruptions of Mount St, Helens through 1982, Science, 221, 1383-1385, 1983.

Casadevall, T. J., J. B. Stokes, L. P. Greenwood, L. L. Malinconico, J. R. Casadevall, and B. T. Furukawa, SO_2 and CO_2 emission rates at Kilauea Volcano, 1979-1984, in *USGS Prof. Paper 1350,* edited by R, Decker, T. Wright, and P. Stauffer, pp. 771-780, 1987.

Char tier, T. A., W. I. Rose, and J. B. Stokes, Detailed record of $S0_2$ emissions from Puu Oo between episodes 33 and 34 of the 1983-1986 ERZ eruption, Kilauea, Hawaii, *Bull. Volcanol., 50,215-228, 1988.*

Doiron, S, D., G. J. S. Bluth, C. C. Schnetzler, A. J. Krueger, and L. S. Walter, Transport of Cerro Hudson $S0_2$ clouds, *EOS Trans. AGU, 72,489-498, 1991.*

Doukas, M.P, and T. M. Gerlach, Sulfur dioxide scrubbing during the 1992 eruptions of Crater Peak, Mount Spurr Volcano, Alaska, in *USGS Bull. 2139,* edited by T.E.C. Keith, pp. 47-57, 1995.

Elias T., A. J. Sutton, and J. B. Stokes, Current $S0_2$ emissions at Kilauea Volcano: quantifying scattered degassing sources, *EOS Trans. AGU, 74, 670-671,* 1993.

Gillespie, A. R., A. B. Kahle, and R. E. Walker, Color enhancement of highly correlated images. I. decorrelation and HSI contrast stretches, *Remote Sens. Environ.,* 20,209-235, 1986.

Good y, R. M., and Y. L. Yung, *Atmospheric Radiation, Second Edition, 519* pp., Oxford Press, New York, 1989.

Heliker C., and T. L. Wright, The PUU Oo-Kupaianaha eruption of Kilauea, *EOS Trans. AGU,* 72, 521-530, 1991.

Hon K., J. Kauahikaua, R. P. Denlinger, and K. MacKay, Emplacement and inflation of pahoehoe sheet flows: observations and measurements of active lava flows on Kilauea Volcano, Hawaii, *Geol. Sot. Am. Bull.,* 106,351-370, 1994.

Kahle, A. B., F. D. Palluconi, S. J. Hook, V. J. Realmuto, and G. Bothwell, The Advanced Spaceborne Thermal Emission and Reflectance Radiometer (ASTER), *Int. J. imaging Sys. Tech., 3, 144-156, 1991.*

Krueger, A. J., Sighting of El Chichón sulfur dioxide clouds with the Nimbus 7 Total Ozone Mapping Spectrometer, Science, 220, 1377-1379, 1983.

Krueger, A. J., L. S. Walter, C. C. Schnetzler, and S. D. Doiron, TOMS measurement of the sulfur dioxide emitted during the 1985 Nevado del Ruiz eruptions, *J. Volcanol. Geotherm. Res., 41,7-15, 1990.*

Krueger A. J., L. S. Walter, P. K. Bhartia, C. C. Schnetzler, N. A. Krotkov, I. Sprod, and G. J. S. Bluth, Volcanic sulfur dioxide measurements from the Total Ozone Mapping Spectrometer (TOMS) instruments, *J. Geophys. Res., 100,14,057-14,076,* 1995.

Kyle, P. R., K. Meeker, and D. Finnegan, Emission rates of sulfur dioxide, trace gases, and metals from Mount Erebus, Antarctic, *Geophys. Res. Let., 17,2125-2128, 1990.*

Kyle, P. R., L. M. Sybeldon, W. C. McIntosh, K. Meeker, and R. Symonds, Sulfur dioxide emission rates from Mount Erebus, Antarctica, in *Antarctic Research Series, Vol 66, Volcanological and Environmental Studies of Mount Erebus, Antarctica, edited* by P.R. Kyle, pp. 69-82, 1994.

McGee, K. A., The structure, dynamics, and chemical composition of noneruptive plumes from Mount St. Helens, 1980-88, *J. Volcanol. Geotherm. Res., 51,269-282, 1992.*

McGee, K. A., and A. J. Sutton, Eruptive activity at Mount St. Helens, Washington, USA, 1984-1988: a gas geochemistry perspective, *Bull. Volcanol.*, 56,433-446, 1994.

Malinconico, L. L., Fluctuations in SO_2 emission during recent eruptions of Etna, *Nature,* 278, 43-45, 1979.

Malinconico, L. L., On the variation of SO_2 emissions from volcanoes, *J. Volcanol. Geotherm. Res.,* 33,231-237, 1987.

Mangan, M. T., C. C. Heliker, T. N. Matttox, J. P. Kauahikaua, and R. T, Helz, Episode 49 of the Puu Oo - Kupaianaha eruption of Kilauea Volcano - breakdown of a steady-state eruptive era, *Bull. Volcanol., 57, 127-135, 1995.*

Mattox T. N., C. Heliker, J. Kauahikaua, and K. Hen, Development of the 1990 Kalapana Flow Field, Kilauea Volcano, Hawaii, *Bull. Volcanol.,* 55,407-413, 1993.

Moffat, A. J., and M. M. Millán, The applications of optical correlation techniques to the remote sensing of SO_2 plumes using sky light, *Atmos. Environ.,* 5, 677-690, 1971.

Newcomb, G. S., and M. M. Millán, Theory, applications, and results of the long-line correlation spectrometer, *IEEE Trans. Geosci. Electron., GE 8, 149-157,* 1970.

Pyle, D, M., P. D. Beattie, and G. J. S. Bluth, Sulphur emissions to the stratosphere from explosive volcanic eruptions, *Bull. Volcanol., 57, 663-671,* 1996.

Realmuto, V. J., M. J. Abrarns, M. F. Buongiornio, and D.C. Pieri, The use of multispectral thermal infrared image data to estimate the sulfur dioxide flux from volcanoes: a case study from Mount Etna, Sicily, July 29, 1986, *J. Geophys. Res.,* 99,481-488, 1994.

Realmuto, V, J., K. Hen, A. B. Kahle, E. A. Abbott, and D. C. Pieri, Multispectral thermal infrared mapping of the 1 October 1988 Kupaianaha flow field, Kilauea Volcano, Hawaii, *Bull. Volcanol., 55,33-44, 1992.*

Rose, W. I., R. L. Chuan, W. F. Giggenbach, P. R. Kyle, and R. B. Symonds, Rates of sulfur dioxide and particle emissions from White Island volcano, New Zealand, and an estimate of the total flux of major gaseous species, Bull. *Volcanol.,* 48, 181-188, 1986.

Rose, W. I., G. Heiken, K. Wohletz, D. Eppler, S. Barr, T. Miller, R. L. Chuan, and R. B, Symonds, Direct rate measurements of eruption plumes at Augustine volcano: a problem of scaling and uncontrolled variables, *J. Geophys. Res., 93,4485-4499, 1988.*

Stephens, G. L., *Remote Sensing of the Lower Atmosphere, 523* pp., Oxford University Press, New York, 1994.

Stoiber, R. E., L. L. Malinconico, and S. N. Williams, Use of the Correlation Spectrometer at Volcanoes, in *Forecasting Volcanic Events,* edited by H. Tazieff and J. C. Sabroux, Elsevier, pp. 425-444, 1983.

Stoiber, R. E., S. N. Williams, and B. Huebert, Annual contribution of sulfur dioxide to the atmosphere by volcanoes, *J. Volcanol. Geotherm. Res., 33, 1-8, 1987.*

Sutton, A. J., T. Elias, and R. Navarrete, The effects of volcanic gas emissions on ambient air character at Kilauea Volcano, Hawaii, *EOS Trans. AGU, 74, 671,* 1993.

Sutton, A. J., K. A. McGee, T. J. Casadevall, and J. B. Stokes, Fundamental volcanic-gas-study techniques: an integrated appraoch to monitoring, *U.S.G.S. Bull. 1966, 181-188, 1992.*

Swanson, D. A., W. A. Duffield, D. B. Jackson, and D, W, Peterson, Chronological narrative of the 1969-71 Mauna Ulu Eruption of Kilauea Volcano, Hawaii, *U.S.G.S. Prof. Paper 10.56,* 1979.

Tilling, R. I., Fluctuations in surface heights of active lava lakes during 1972-1974 Mauna Ulu eruption, Kilauea Volcano, Hawaii, *J. Geophys. Res.* 92, 13,721-13,730, 1987.

Walter, L. S., G. J. S. Bluth, C. C. Schnetzler, I. E. Sprod, and A. J. Krueger, Satellite observations of $S0_2$ emissions from the 1984 Mauna Loa eruption. *EOS Trans. AGU 74, 636, 1993.*

Wolfe, E.W. (cd.), The Puu Oo eruption of Kilauea Volcano, Hawaii: episodes 1 through 20, January 3, 1983, through June 8, 1984, *U.S.G.S. Prof. Paper 1463, 1988.*

Zreda-Gostynska G., and P. R. Kyle, Chlorine, fluorine, and sulfur emissions from Mount Etna, Antarctica, and estimated contributions to the antarctic atmosphere. *Geophys. Res. Let.* 20, 1959-1962, 1993.

Captions for Realmuto et al., Multispectral imaging of Sulfur Dioxide...

Figure 1. Locations of the Pu'u 'O'o and Kupaianaha vents relative to the summits of Kilauea and Mauna Loa Volcanoes and the city of Hilo. Also shown are the boundaries of the Puu Oo and Kupaianaha lava flow fields as of September 30, 1988 [*Realmuto et al.,* 1992].

Figure 2. Comparison of the spectral transmission of two 1.05 km atmospheric columns, as calculated with MODTRAN. The inputs to MODTRAN included the Hilo radiosonde data and plume dimensions calculated from cloud shadows (cf. Table 1). The plot depicts the ratio of the transmission through a column containing 0.1 g m^{-2} SO_2 to that of a column containing no SO_2 as a heavy line. The transmission ratio is superimposed on the normalized spectral response functions of the six TIMS Channels (as of December, 1987), which are depicted as shaded regions.

Figure 3. Sensitivity of SO_2 column abundance estimates to uncertainties in the (a) midpoint altitude and (b) thickness of the Pu'u 'O'o plume.

Figure 4. Total SO_2 burden levels derived from an HVO COSPEC survey of Pu'u 'O'o on September 20, 1988.

Figure 5. MODTRAN simulation of the apparent changes in ground temperature (relative to 304 K) perceived by ASTER as it views the ground through the Pu'u 'O'o plume (see Table 1 for plume dimensions). The Hilo radiosonde data were used to describe the atmospheric column up

to 10 km and the MODTRAN tropical atmosphere model was used for the remainder. The broken line represents a column abundance of 5 g m^{-2}, the dashed line 10 g m^{-2}, and the solid line 15 g m^{-2}.

Plate 1. NSOO1 image data acquired over the East Rift Zone study site on September 30, 1988. Color composites of data from the (a) visible and (b) short wavelength infrared (SWIR) channels. Note locations of Pu'u 'O'o and Kupaianaha vents, skylight fumarole, and the meteorologic clouds that overlaid the Pu'u 'O'o $S0_2$ plume.

Plate 2. TIMS image data acquired over the East Rift Zone study site on September 30, 1988. Color-composite of data from TIMS Channels 5,3, and 2 (cf. Fig. 2) displayed in red, green, and blue, respectively.

Plate 3. Pu'u 'O'o SO_2 column abundance map, contoured to an interval of 2 g m^{-2}. Scale bar indicates the color code of each contour level. A, B, C, and D identify the transect lines across which the $S0_2$ cross-section of the plume was estimated (cf. Table 2).

Plate *4.* Pu'u 'O'o ground temperature map, contoured to an interval of 2 K. Scale bar indicates the color code of each contour level. Note the ground temperature anomalies associated with the high concentration puffs revealed in Plate 3.

Plate 5. Kupaianaha $S0_2$ column abundance map, contoured to an interval of 1 g m^{-2}. Scale bar indicates the color code of each contour level. A, B, and C identify the transect lines across which

the SO_2 cross-sections of the plumes were estimated (cf. Table 2). Transect C intersects the sky-light plume.

Plate 6. Kupaianaha ground temperature map, contoured to an interval of 2 K. Scale bar indicates the color code of each contour level.

Plate 7. Pu'u 'O'o SO_2 column abundance map (Plate 3), resampled to the 90 m spatial resolution of ASTER. Map is contoured to an interval of 2 g m^{-2}, with the color code of each contour level indicated by the scale bar. Note that the four puffs revealed in Plate 3 can still be recognized at this lower spatial resolution.

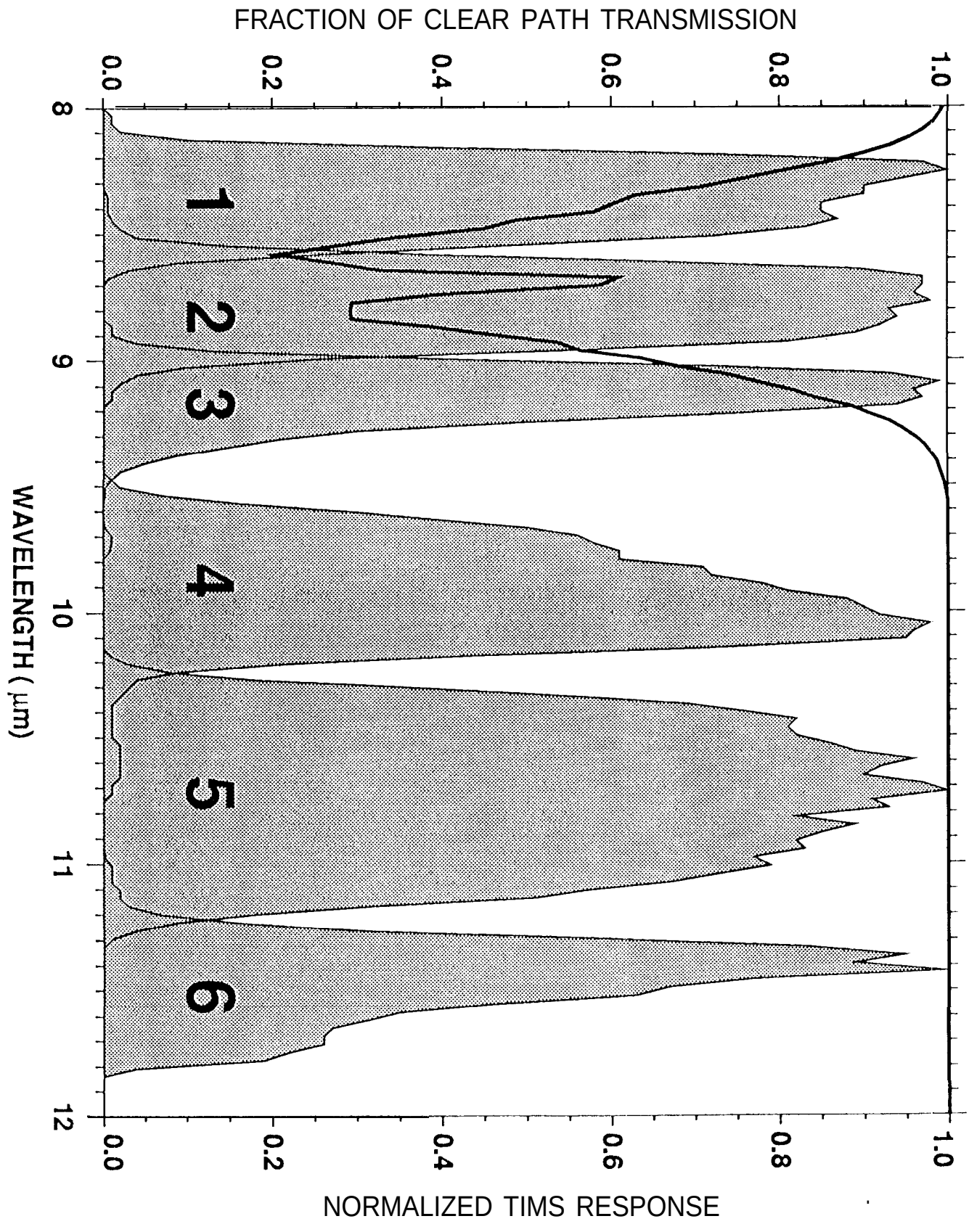
FRACTION OF CLEAR PATH TRANSMISSION
0.0
0.2
0.4
0.6
0.8
1.0
8
9
10
11
12
WAVELENGTH (μm)
1
2
3
4
5
6
0.0
0.2
0.4
0.6
0.8
1.0
NORMALIZED TIMS RESPONSE

Fig. ~~Plate~~ 2

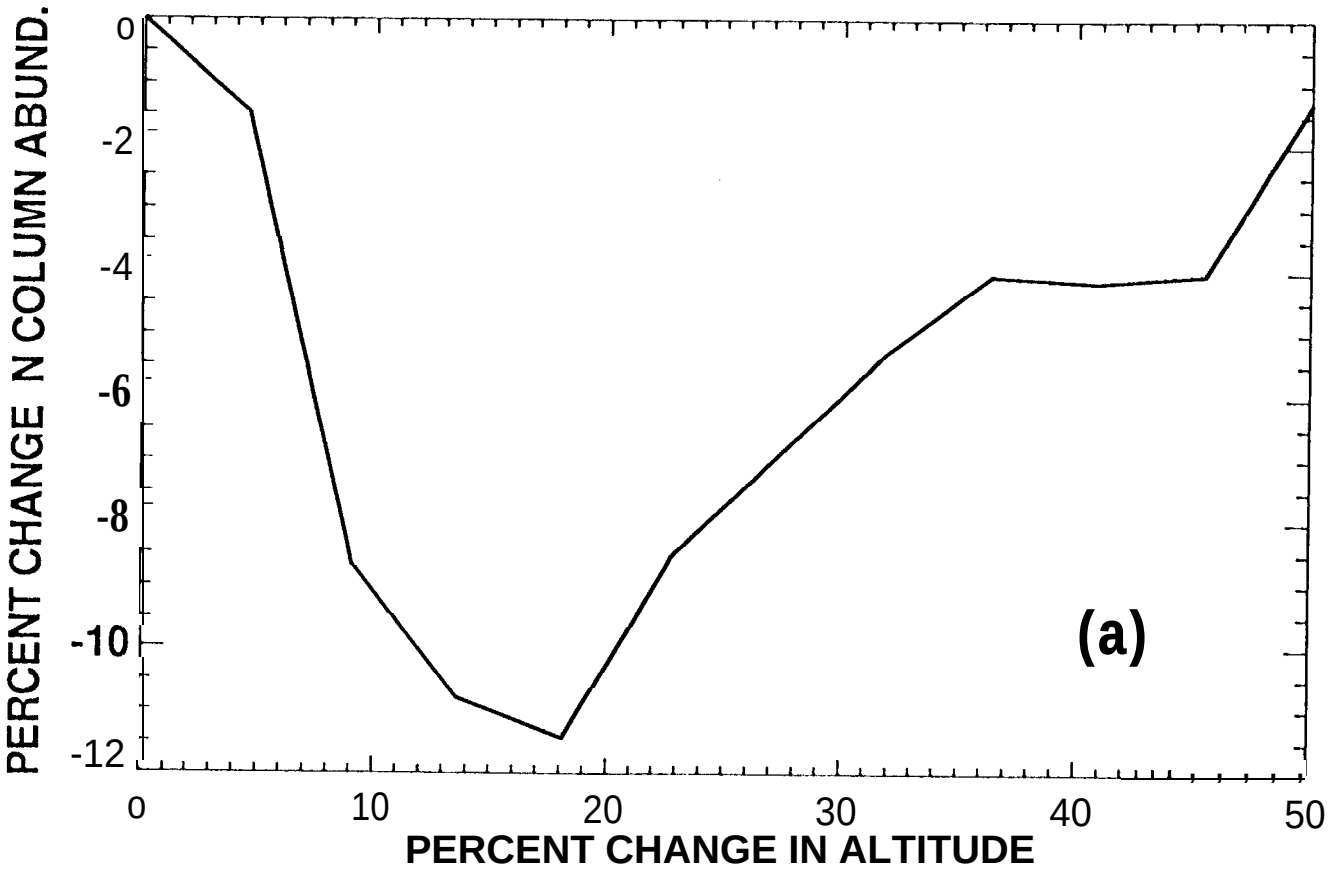
PERCENT CHANGE N COLUMN ABUND.
0
-2
-4
-6
-8
-10
-12
0
10
20
30
40
50
PERCENT CHANGE IN ALTITUDE
(a)

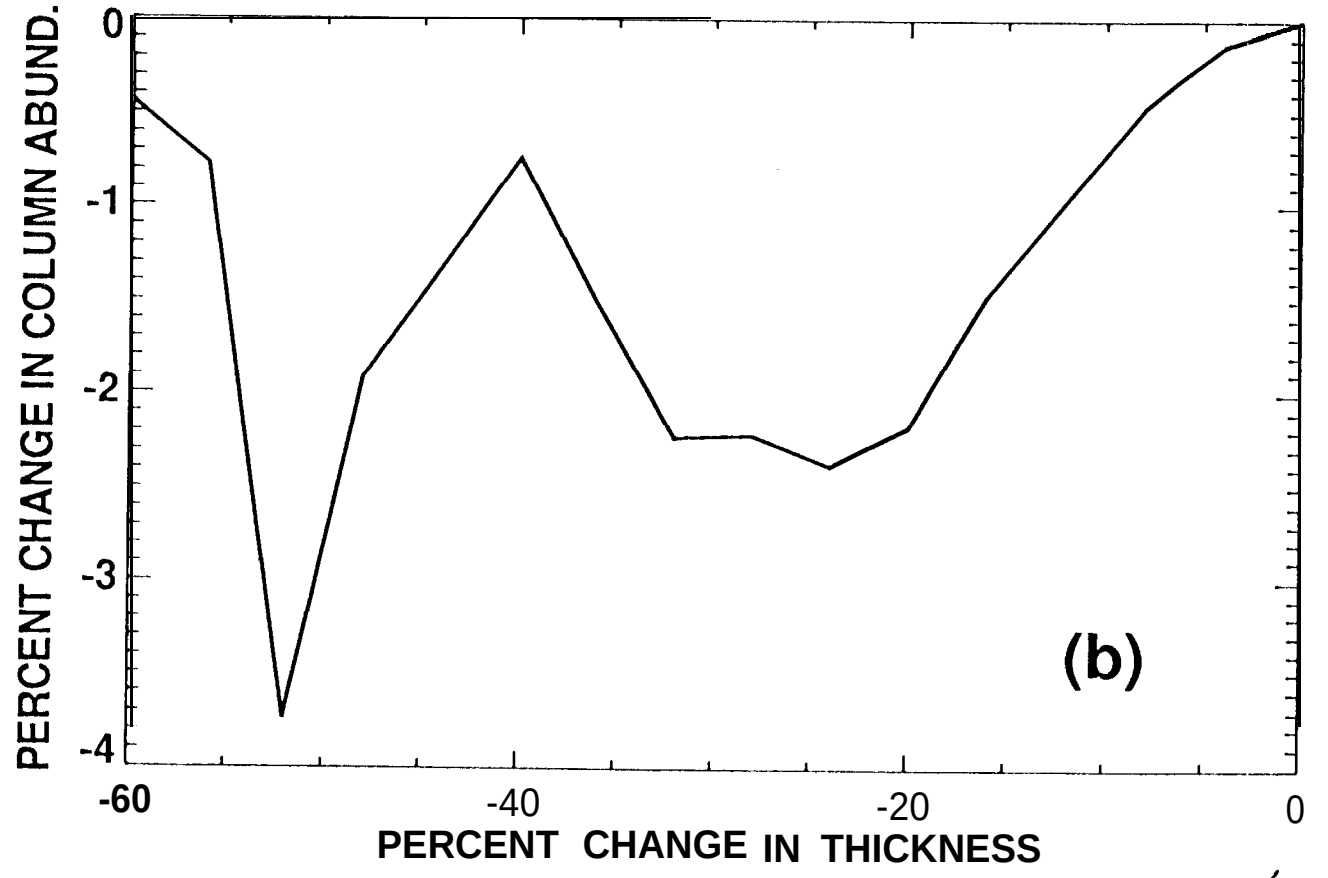
PERCENT CHANGE IN COLUMN ABUND.
0
-1
-2
-3
-4
-60
-40
-20
0
PERCENT CHANGE IN THICKNESS
(b)

Fig 3

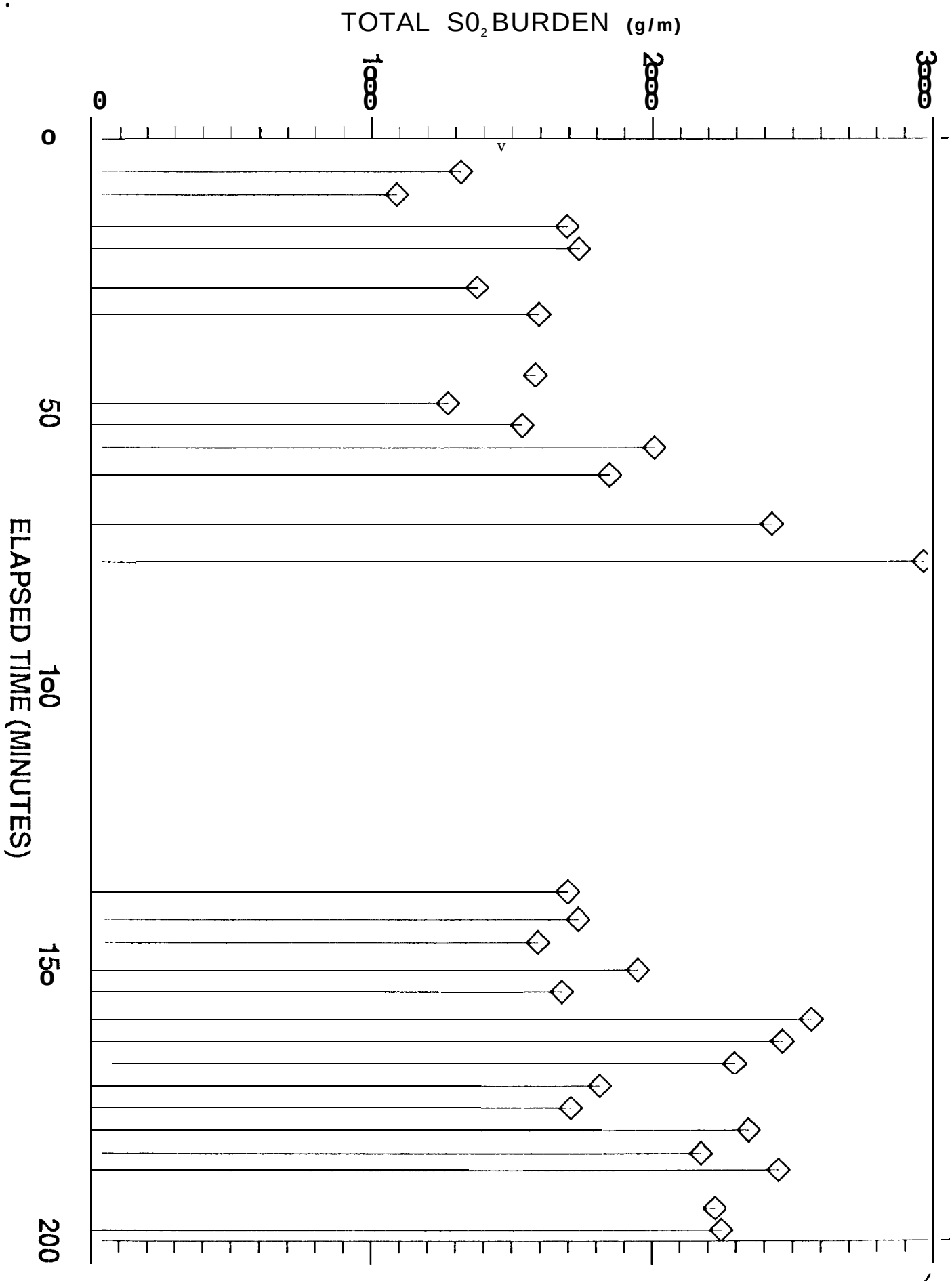
TOTAL SO_2 BURDEN (g/m)
0
1000
2000
3000
0
50
100
150
200
ELAPSED TIME (MINUTES)

Fig. 4

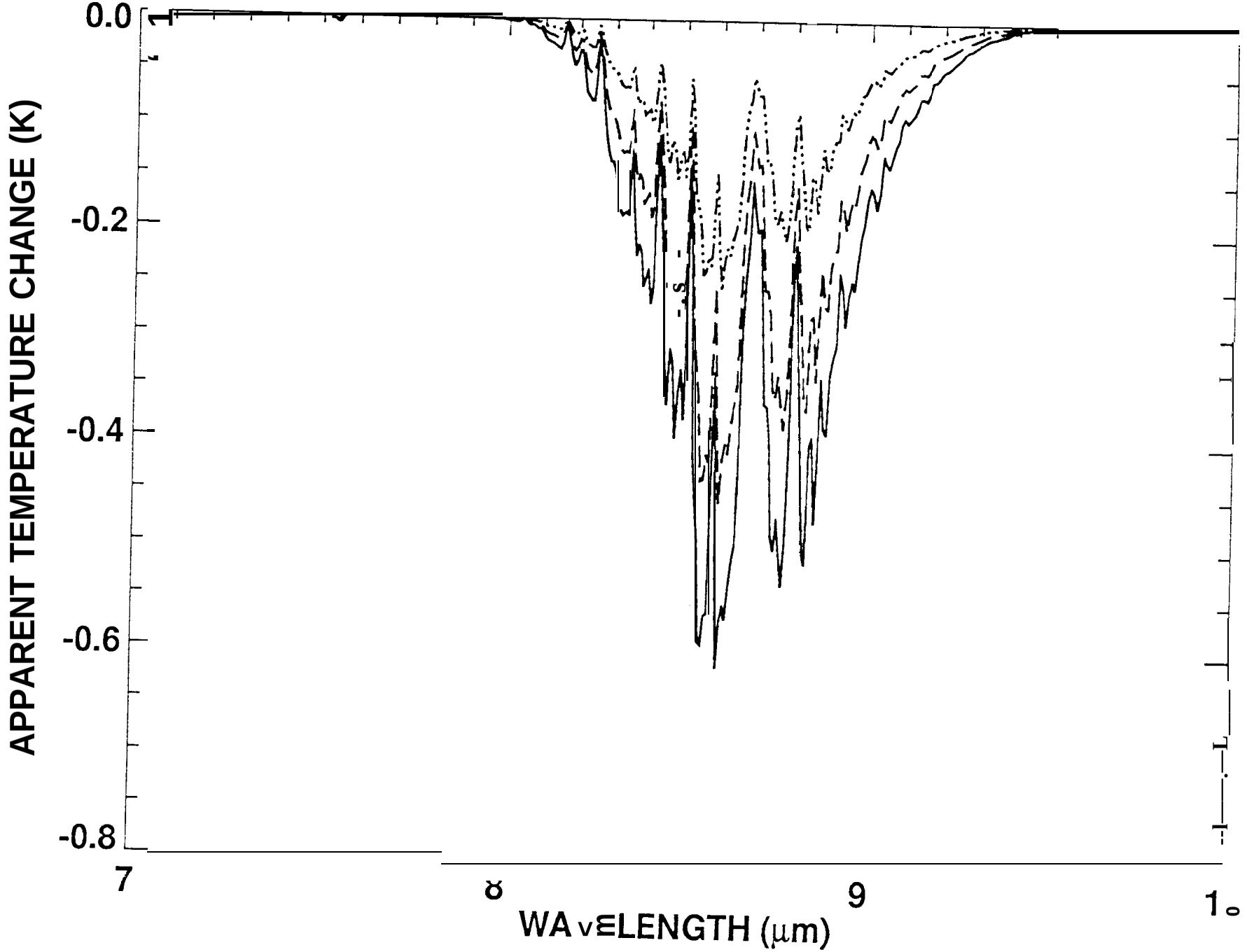
0.0
-0.2
-0.4
-0.6
-0.8
APPARENT TEMPERATURE CHANGE (K)
7
8
9
10
WAVELENGTH (μm)

Fig. 5

Plate 1

Plate 2

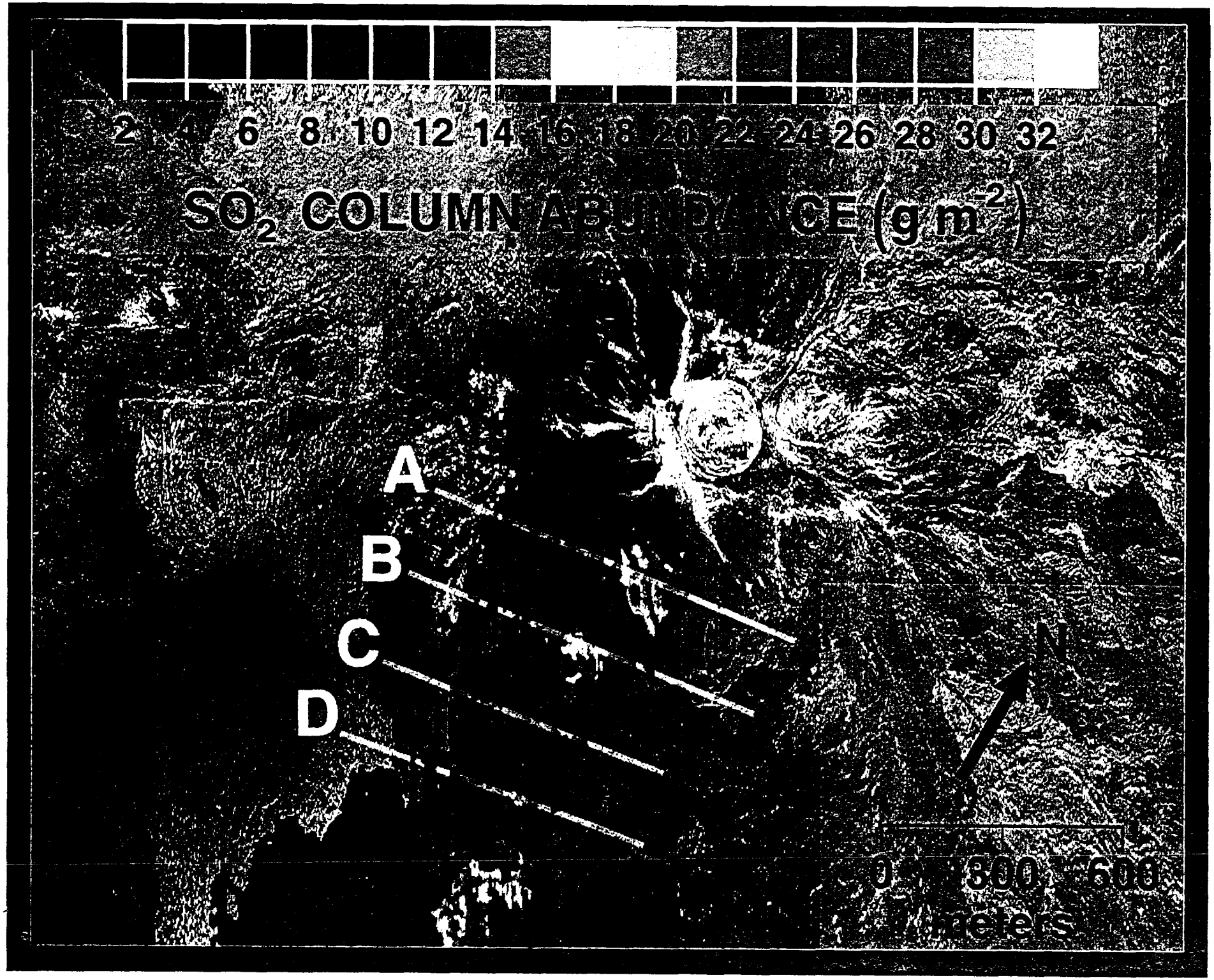
2 4 6 8 10 12 14 16 18 20 22 24 26 28 30 32
SO_2 COLUMN ABUNDANCE ($g\ m^{-2}$)
A
B
C
D
N
0 800 1600
Meters

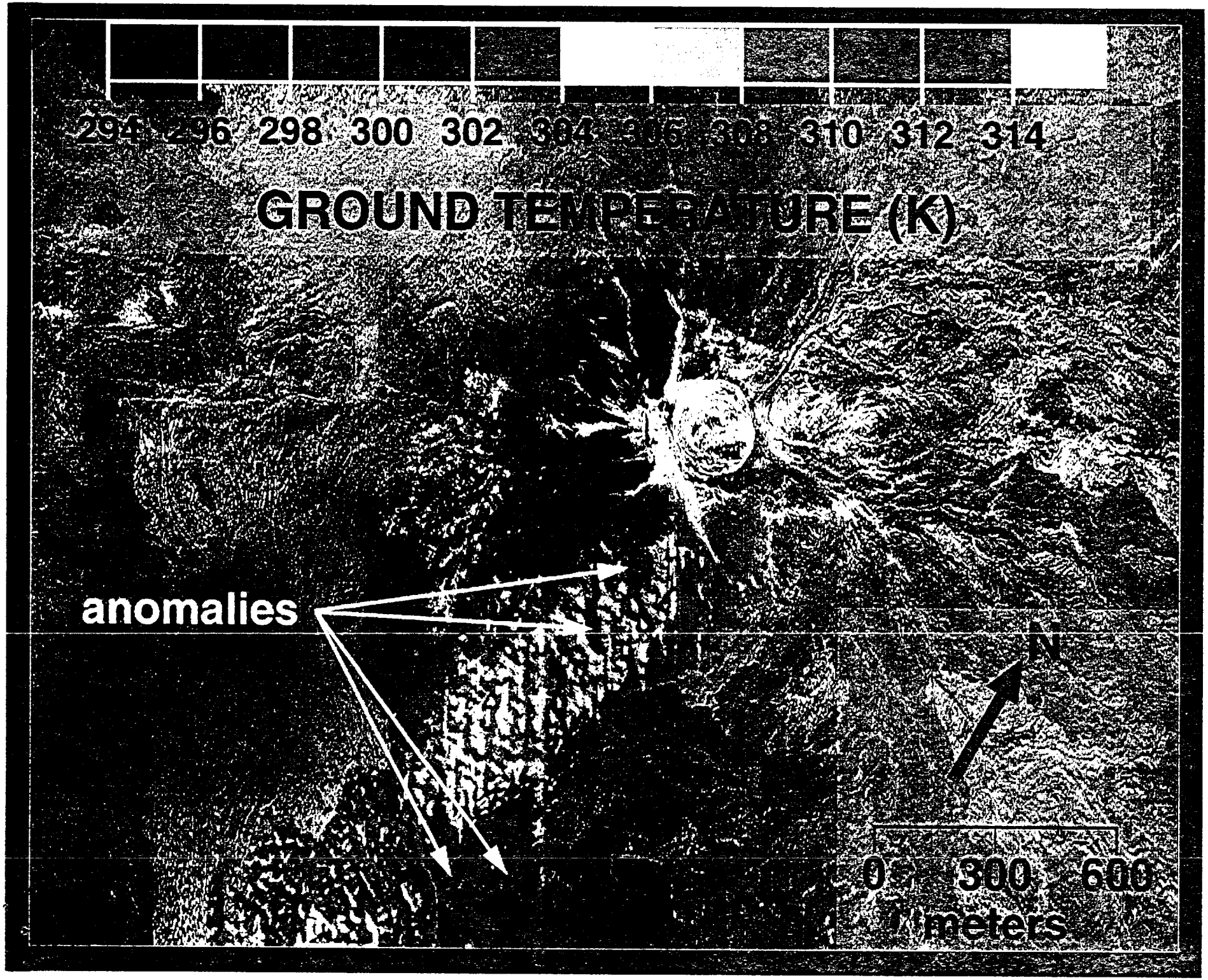
294 296 298 300 302 304 306 308 310 312 314
GROUND TEMPERATURE (K)
anomalies
N
0 300 600
meters

Plate 11

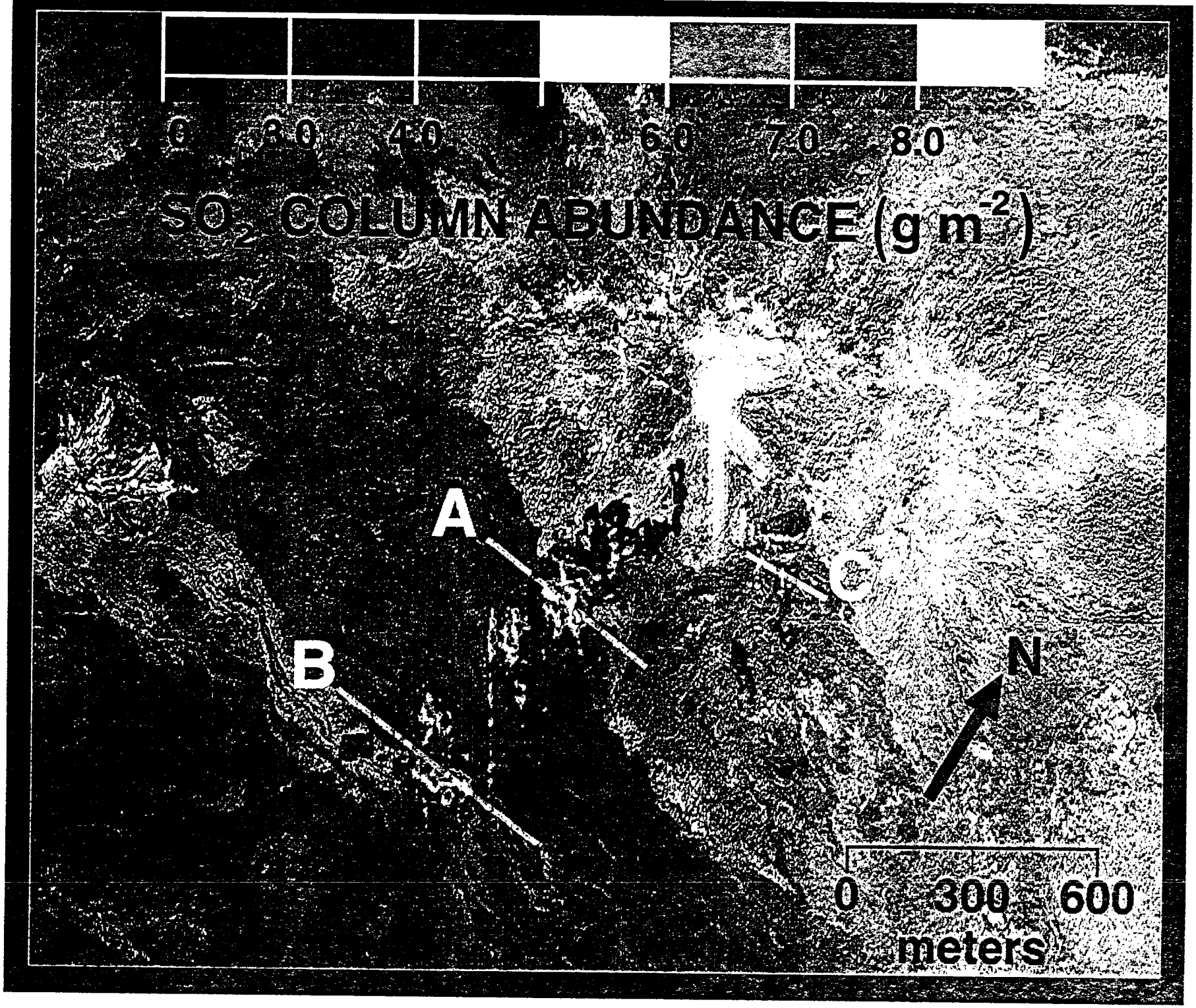

Plate 5


298 300 302 304 306 308 310 312 314 316
GROUND TEMPERATURE (K)
N
0 300 600
meters

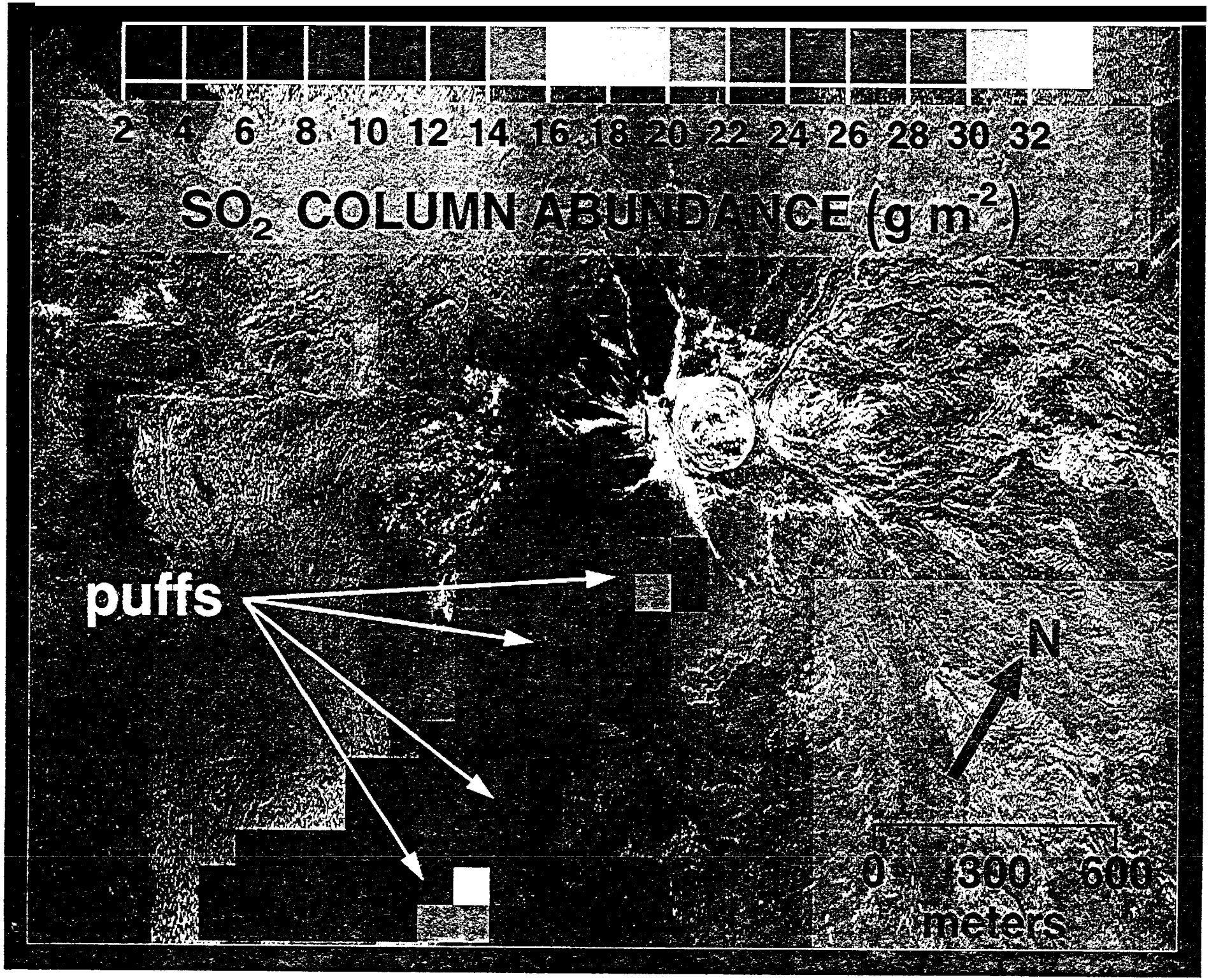
2 4 6 8 10 12 14 16 18 20 22 24 26 28 30 32
SO_2 COLUMN ABUNDANCE ($g\ m^{-2}$)
puffs
N
0 300 600
meters

Plate 7

'l'able 1. Plume Dimensions Submitted to MODTRAN

Plume	Midpoint Altitude (km)	Thickness (km)	Ground Elevation (km)	Sensor Altitude (km)
Pu'u '0'0	1.100	0.250	0.850	1.900
Kupaianaha	0.900	0.060	0.760	1.900
Skylight	0.900	0.100	0.760	1.900

Table 2. Calculated SO_2 Emission Rates for the Pu'u 'O'o, Kupaianaha, and Skylight Vents

Vent	Transect	Total Burden of SO_2	SO_2 Emission Rate	
		(g/m)	(kg/s)	(t/d)
Pu'u '0'0	A	5176	25.9 -31.1	2238-2687
(cf. Plate 3)	B	3763	18.8 -22.6	1624-1953
	c	1989	9.9- 11.9	855-1028
	D	2505	12.5 -15.0	1080-1296
Kupaianaha	A	1173	5.9- 7.0	510-605
(cf. Plate 5)	B	1340	6.7- 8.0	579-691
Skylight	c	271	1.4- 1.6	121-138
(cf. Plate 5)				